Materials Research Proceedings 69 (2026) 48-53 https://doi.org/10.21741/9781644904251-9

Lunar Descent and Landing Via Fusion of Deep Learning-Based Visual Navigation and Moonlight Signals

Michele CERESOLI[1,a,*], Floor MELMAN[2], Yoann AUDET[2], Richard SWINDEN[2], Francesco CAPOLUPO[2] and Michèle LAVAGNA[1]

[1]Department of Aerospace Science and Technology, Politecnico di Milano, Via La Masa 34, 20156, Milan, Italy

[2]European Space Research and Technology Centre (ESTEC), European Space Agency, Keplerlaan 1, 2201AZ, Noordwijk, The Netherlands

[a]michele.ceresoli@polimi.it

Keywords: Lunar Landing, Vision-Based Navigation, Moonlight, Deep-Learning

Abstract. The renewed momentum in lunar exploration has driven the development of dedicated lunar communication and navigation infrastructures such as the European Space Agency's Moonlight Lunar Communication and Navigation System (LCNS). In this context, landing operations are key mission phases that enable humans and scientific experiments to reach the Moon surface. However, recent crashes of both public and private missions have highlighted how challenging and complex such operations are. As such, this work investigates the achievable navigation performance of a lunar lander targeting the Moon's South Pole through the integration of One-Way Ranging signals from LCNS and Deep Learning–based Vision-Based Navigation measurements, showcasing the benefits that the fusion of these two distinct type of measures can bring.

Introduction

Planetary landings represent a very challenging scenario for Guidance, Navigation and Control (GNC) systems. Indeed, due to a combination of fast-landing dynamics, communication delays, and restricted coverage of landing areas, real-time ground control is often limited or impractical. Recent attempts to land on the lunar surface have further highlighted the need for an autonomous and reliable GNC module. Thus, to support these missions, the European Space Agency (ESA) is currently developing the Moonlight Lunar Communication and Navigation System (LCNS) that will provide GNSS-like signals enabling One-Way Ranging (OWR) for future lunar users. However, as the constellation will be gradually deployed, an initial key challenge will be the limited availability of such signals with respect to well-established Earth GNSS systems. Within this context, current and future landing missions rely on Vision-Based Navigation (VBN) techniques to estimate the state of the lander while minimizing the overall size, weight and power of the GNC subsystem. As such, this study aims to showcase the performance and robustness improvements that the integration of radiometric OWR signals with AI-based VBN techniques can bring to landing vehicles.

Landing Trajectory

The considered mission scenario consists in the spacecraft descent from the pericenter of an elliptical Low Lunar Orbit (LLO) (100×30 km altitude) to touchdown at a targeted landing site close to the Lunar South Pole. The trajectory reproduces the common scheme of lunar landings and begins with the Main Braking Burn (MBB), where the engines are initiated at full thrust to reduce the orbital velocity. This maneuver lasts until the lander reaches the Pitch-Up Gate (PGA), at an altitude of about 1 km, where thrust is re-oriented towards the vertical direction and the Hazard Detection and Avoidance (HDA) sensors and routines are activated. A final powered descent is foreseen for the last few hundreds of meters and ends before the final vertical descent at the Vertical Gate (VGA), where the horizontal velocity becomes null.

The trajectory was generated following the expected profile of the Argonaut mission [1], using an indirect optimization technique for the main braking phase, and a semi-analytical guidance for the final approach [2]. The lander is assumed to have an initial mass of 7000 kg, a maximum thrust of 18000 N, and a specific impulse of 330s. The entire descent duration is of 584s. The target landing site has been selected near the Sverdrup crater, in proximity of the South Pole, at approximately 153° W and 88° S.

The dynamical model used to simulate the true lander dynamics includes most of the major perturbations that are relevant in a lunar scenario and that affect the navigation accuracy. Specifically, it accounts for the gravitational point-mass accelerations due to the Earth, Sun and Moon as well as the effects of the irregular lunar gravity field. The latter are modelled using a spherical harmonic expansion up to 120×120 degree and order. On the other hand, control errors are assumed null.

On-board Sensors

The lander is equipped with a monocular camera to acquire navigation images and with two antennas to retrieve the LCNS signals. An Inertial Measurement Unit (IMU) is instead used to retrieve both acceleration and angular velocity readings. Finally, a star tracker enables precise attitude measurements, with an accuracy up to 10 arcseconds. A brief overview of the mathematical modeling of each sensor is provided hereafter.

Inline with previous work [3], the LCNS constellation is comprised of 4 satellites deployed on 4 distinct Elliptical Lunar Frozen Orbits (ELFO). The constellation parameters are based on internal Moonlight studies and are designed to optimize the South Pole visibility. All satellites are deployed on orbits with a 24-hours orbital period and a nominal eccentricity of 0.63.

The Signal-in-Space Error (SISE) is modeled using a realistic Orbit Determination and Time Synchronization (ODTS) simulator [4], which provides the time series of the errors in each satellite's position, velocity, and clock states. The user on-board clock is modelled using a two-state clock model, in which the frequency deviation is originated from two types of noise, a White Frequency Modulation (WFM) and a Random Walk Frequency Modulation (RWFM). The standard deviations of the noises are based upon a space-qualified OCXO, inline with previous studies [3]. The LCNS receiver is designed to track the LunaNet AFS signal specifications using Delay Locked Loop (DLL) and Frequency Locked Loop (PLL) techniques, providing as an output the pseudorange and doppler quantities with respect to each visible LCNS satellite. The standard DLL and FLL equations are used to characterize the pseudorange and measurement noises. The patterns for the transmitting and receiving antennas are also based upon the on-going Moonlight studies [3,4].

A high-fidelity model is used to account for the measurement errors that real IMUs are subject to, including non-orthogonalities, scale factor, bias and noise errors. The parameters are loosely based upon the flight-proven LN-200HPS model from Northrop Grumman.

A monocular camera is installed on the side of the lander, at angle of 22.5° with respect to the face normal, ensuring constant visibility of the Moon surface throughout the spacecraft descent. The camera is based upon the standard pinhole model, with a 640×640 resolution and a Field-of-View (FOV) of 45°. Images of the Moon surface are generated using the in-house rendering software presented in [5]. Two distinct pipelines are used to process the acquired images.

Navigation Filter Architecture

The navigation module consists of an Extended Kalman Filter (EKF) to estimate the absolute inertial position and velocity of the lander together with the LCNS OWR receiver clock bias and drift, and a Multiplicative Extended Kalman Filter (MEKF) to estimate the lander inertial attitude and gyroscope bias. An overview of the entire navigation module is given by Figure 1.

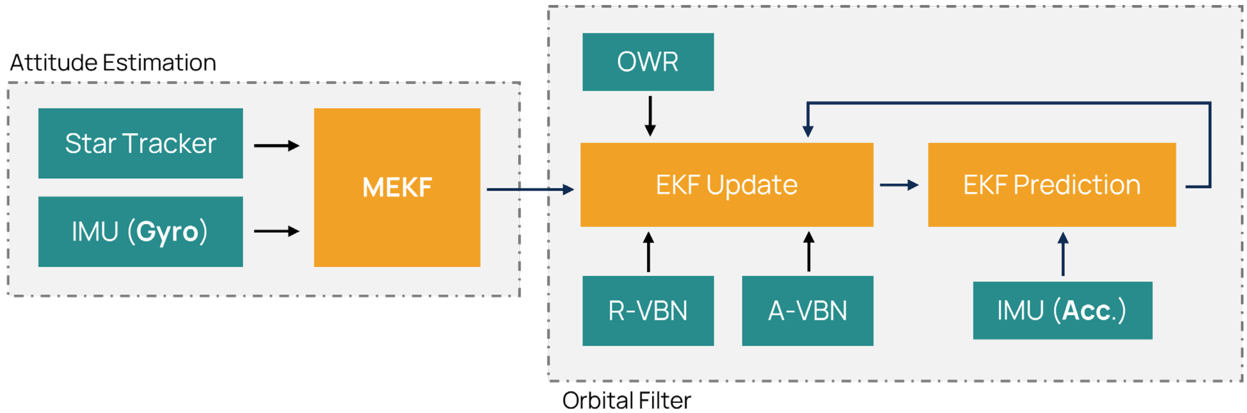

Figure 1: High-level overview of the navigation block interfaces.

The Absolute Vision Based Navigation (A-VBN) module uses Moon impact craters as landmarks, comparing them with a dedicated on-board crater catalogue to retrieve absolute estimates of the lander position. The adopted catalogue is derived from the global Robbins catalogue [6], which has been expanded by manually mapping all the visible craters along the expected spacecraft groundtrack. A Deep Neural Network (DNN) based upon the YOLOv11n architecture is used to identify the bounding box surrounding each crater. Subsequently the crater shape is fitted with an ellipse and matched against the crater database to retrieve its selenographic coordinates. The crater matching algorithm is based upon an iterative direct matching strategy, which leverages the estimated spacecraft position and orientation to project onto the image plane the on-board catalogue. Detected and projected craters are then transformed into bivariate Gaussian Probability Density Functions (PDFs), and their similarity is quantified through the Gaussian Angle distance. A RANSAC-based outlier rejection strategy is then used to identify potential wrong matches. Finally, the resulting pairs of detected and projected craters are used to assemble a Perspective-n-Crater (PnC) problem, which leverages the known spacecraft orientation and the full information from the crater shapes to compute an estimate of the spacecraft position with respect to the Moon-fixed frame [7]. The M-estimator SAmple Consensum (MSAC) algorithm is used to further mitigate the impact of outliers.

On the other hand, the Relative Vision Based Navigation (R-VBN) module integrates multiple-view geometry and deep-learning to estimate the direction of motion of the lander from one image frame to the other. It leverages SuperPoint, a deep-learning based feature extractor [8] to identify 2D features in the images, which are then matched using a brute-force approach. Using the known spacecraft attitude a system of equations enforcing the epipolar constraint is then assembled and solved for the relative camera translation direction [7]. To enhance robustness, MSAC is again adopted to reject potential outliers from the identified 2D features pairs.

Both the EKF and the MEKF filters are executed at 10 Hz, with the IMU measurements sampled at the same frequency. On the other hand, due to the post-processing requirements, the A-VBN position estimate is assumed to be available at a frequency of 0.1 Hz and with a delay of 10s (i.e., the measurement at time *k* is associated to the pose the spacecraft had 10 seconds before *k*), while the R-VBN measures are given at a frequency of 0.5 Hz. Finally, the OWR pseudorange and

Materials Research Proceedings 69 (2026) 48-53 https://doi.org/10.21741/9781644904251-9

Doppler signals are ingested at 1 Hz and fused using a tightly-coupled approach. Stochastic Cloning (SC) is used to handle both delayed and relative measurements by making two independent copies of the position states, each synchronized to the associated measurement. A simplified dynamic model is used to predict the inertial position and velocity of the lander, which uses a 40×40 expansion of the Moon gravity field. For the process noise, the global contribution of unmodelled dynamic accelerations and IMU biases is assumed to behave as a First-Order Gauss-Markov (FOGM) processes, following the Dynamic Model Compensation (DMC) algorithm. On the other hand, the process noise of the clock states assumes the clock drift is also driven by a FOGM, while the clock bias is the integral of the drift plus a Gaussian noise term.

Results and Discussion

A Montecarlo simulation with 200 samples has been performed for two distinct scenarios, with 2 and 3 visible LCNS satellites, respectively. The results in terms of 3D position error are reported in Figure 2. In both cases the final navigation error is very small, under 7m (99th) with 2 satellites and smaller than 5m (99th) with 3. A comparison between the two also highlights a faster convergence when 3 satellites are available, as well as the maximum error being smaller than 40m with respect to the 50m achieved when only 2 LCNS signals are tracked.

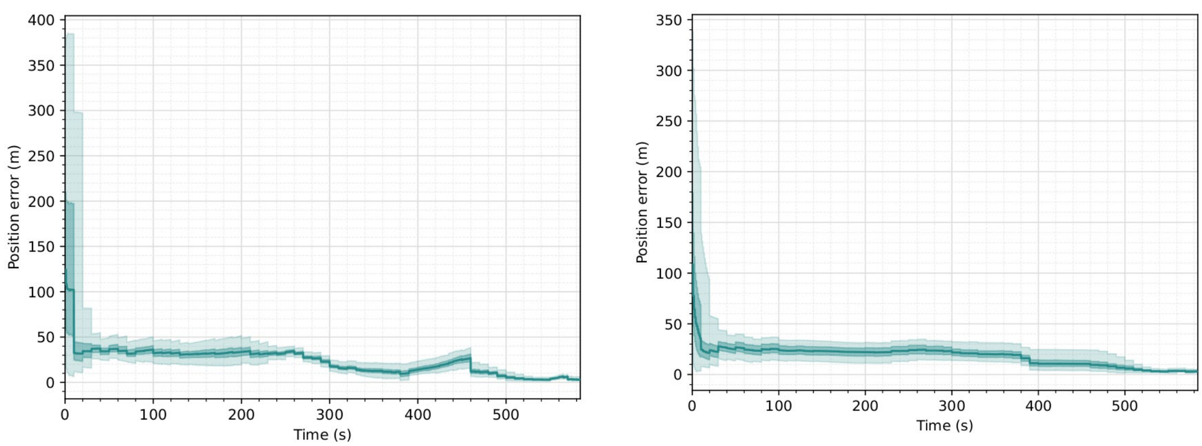

Figure 2: 3D position error throughout the descent with 2 (left) and 3 (right) LCNS satellites in visibility

The benefits of merging VBN and OWR measurements can be further appreciated by comparing the results in Figure 2 with those in Figure 3, which reports the Montecarlo simulations when VBN-only measures are considered. Indeed, despite the VBN-only solution already provides a satisfactory final navigation error below 20m (99th), the addition of OWR measurements further improves this result, reducing the maximum navigation error after the initial convergence from 100m to around 50m. Moreover, these added signals can also prove beneficial when above areas that are either not covered by the on-board crater catalogues or are characterized by unfavorable illumination conditions, scenarios in which the VBN may struggle to provide meaningful measures.

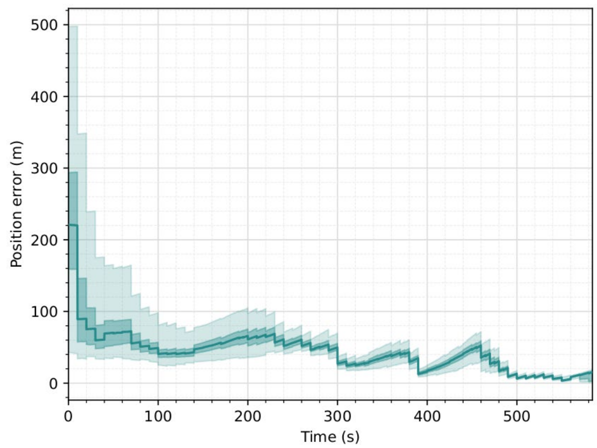

Figure 3: 3D position error throughout the descent trajectory with VBN-only measurements

On the other hand, it is well known that for OWR measures, a minimum of 4 visible satellites is requested to compute a position-fix. In this regard, these simulations highlight that the addition of VBN measurements allows a stable navigation solution to be computed even with limited LCNS availability.

Conclusions

The International Space Exploration Coordination Group (ISECG) has quantified 90m as a threshold for the maximum landing uncertainty with respect to the target location that guarantees the safety of the operations. This contribution shows that the fusion of vision-based and radiometric data from the proposed LCNS constellation is capable of meeting this strict navigation requirement over a candidate landing site at the Lunar South Pole. Moreover, it highlights the robustness of the solution even when only a portion of the LCNS satellites is visible.

References

[1] F. Capolupo, A. Rinalducci, Descent & Landing Trajectory Guidance Algorithms with Divert Capabilities for Moon Landing, AIAA Scitech Forum, 2024 https://doi.org/10.2514/6.2024-0086

[2] P. Lunghi, P. Di Lizia, R. Armellin, M. Lavagna, Semi-analytical adaptive guidance computation for autonomous planetary landing.

[3] Y. Audet, M. Ceresoli, F. Melman, D. Psychas, R. Swinden, C. Stallo, J. Ventura-Traveset, Assessment of lunar users' PVT performances tightly coupling Moonlight signal with IMU, MDPI (2025)

[4] Y. Audet, F. Melman, D. Psychas, R. Swinden, J. Ventura-Traveset, Positioning of a Lunar Lander Using a Dedicated Lunar Communication and Navigation System Assuming Realistic ODTS Performances, Engineering Proceedings, MDPI (2025) https://doi.org/10.3390/engproc2025088074

[5] M. Ceresoli, S. Silvestrini, M. Lavagna, Optical Image Generation Through Digital Terrain Models for Autonomous Lunar Navigation, Aerospace, MDPI (2025) https://doi.org/10.3390/aerospace12020092

[6] S. Robbins, A new global database of lunar impact craters¿ 1-2 km, Journal of Geophysical Research: Planets, Wiley Online Library, 2019, pp. 871-892 https://doi.org/10.1029/2018JE005592

Materials Research Proceedings 69 (2026) 48-53 https://doi.org/10.21741/9781644904251-9

[7] J. Christian, H. Derksen, R. Watkins, Lunar crater identification in digital images, The Journal of Astronautical Sciences, Springer, 2021, pp. 1056-1144 https://doi.org/10.1007/s40295-021-00287-8

[8] D. DeTone, T. Malisiewicz, A. Rabinovich, Proceedings of the IEEE conference on computer vision and pattern recognition workshop, 2018, pp. 224-236.